BIOCHEMISTRY
including biophysical chemistry & molecular biology

Article

pubs.acs.org/biochemistry

Structural Studies of the Molybdenum Center of Mitochondrial Amidoxime Reducing Component (mARC) by Pulsed EPR Spectroscopy and ^{17}O-Labeling

Asha Rajapakshe,[‡] Andrei V. Astashkin,[‡] Eric L. Klein,[‡] Debora Reichmann,[§] Ralf R. Mendel,[§] Florian Bittner,[§] and John H. Enemark*[,‡]

[‡]Department of Chemistry and Biochemistry, The University of Arizona, Tucson, Arizona 85721, United States

[§]Department of Plant Biology, Technische Universität Braunschweig, Braunschweig, Germany

Supporting Information

ABSTRACT: Mitochondrial amidoxime reducing components (mARC-1 and mARC-2) represent a novel group of Mo-containing enzymes in eukaryotes. These proteins form the catalytic part of a three-component enzyme complex known to be responsible for the reductive activation of several *N*-hydroxylated prodrugs. No X-ray crystal structures are available for these enzymes as yet. A previous biochemical investigation [Wahl, B., et al. (2010) *J. Biol. Chem., 285*, 37847−37859] has revealed that two of the Mo coordination positions are occupied by sulfur atoms from a pyranopterindithiolate (molybdopterin, MPT) cofactor. In this work, we have used continuous wave and pulsed electron paramagnetic resonance (EPR) spectroscopy and density functional theoretical (DFT) calculations to determine the nature of remaining ligands in the Mo(V) state of the active site of mARC-2. Experiments with samples in D_2O have identified the exchangeable equatorial ligand as a hydroxyl group. Experiments on samples in $H_2{}^{17}O$-enriched buffer have shown the presence of a slowly exchangeable axial oxo ligand. Comparison of the experimental ^{1}H and ^{17}O hyperfine interactions with those calculated using DFT has shown that the remaining nonexchangeable equatorial ligand is, most likely, protein-derived and that the possibility of an equatorial oxo ligand can be excluded.

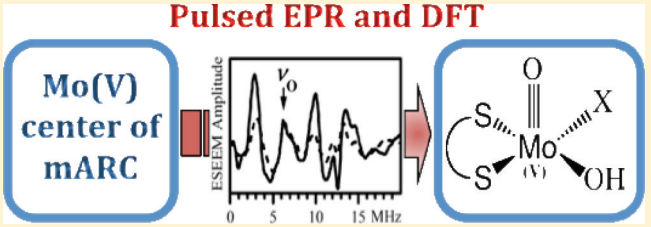

Molybdoenzymes play key roles in the metabolism of virtually all organisms.[1−3] They catalyze reactions involving transfer of an oxygen atom to or from the substrate in global carbon, nitrogen, and sulfur cycles. Hille classified mononuclear Mo-containing enzymes into three families—xanthine oxidase (XO), dimethyl sulfoxide reductase (DMSOR), and sulfite oxidase (SO)—based on the structure of the active site and the amino acid sequence.[1,4,5] A molybdenum cofactor (Moco), a complex of oxidized molybdenum with one or two pyranopterindithiolate (molybdopterin, MPT) ligands, is common among all of these families. The recently discovered mitochondrial amidoxime reducing component (mARC) enzyme is the fourth Mo enzyme found in humans, which remarkably could not be grouped into any of the known Mo enzyme families.[6−10] In fact, mARC proteins share a significant degree of sequence similarity to the C-terminal domains of eukaryotic Moco sulfurases, which are required for a Moco-dependent post-translational activation of enzymes of the XO family.[11] According to the presence of a conserved cysteine, Moco sulfurases and mARC proteins were presumed to form the new "Moco sulfurase C-terminal domain-containing" (MOSC) protein family with a predicted function of the conserved cysteine in sulfur transfer reactions.[12] The function of Moco sulfurases is indeed to transfer a sulfur atom to the Mo center of XO family enzymes; however, this function can be excluded for mARC enzymes because a deficiency in the Moco sulfurase gene alone causes the total loss of activity in XO family enzymes.[11,13,14]

The mARC enzymes represent the catalytic part of a three-component N-reductive system, together with cytochrome b_5 (cyt b_5) and cytochrome b_5 reductase (cyt b_5R). The mARC enzymes are also the first eukaryotic molybdoenzymes that possess separate electron transport proteins. The native enzyme from the pig liver mitochondria was found to be capable of activating *N*-hydroxylated prodrugs by reducing inactive amidoxime prodrugs to the corresponding active amidine groups.[7] Since then, both native and recombinant mARC proteins have been shown to have capabilities to activate *N*-hydroxylated compounds, which are often used in medical applications as prodrugs. Prodrugs have attracted major attention in drug design and development. For example, 19.4% of all small molecular weight drugs approved in the period from 2000 to 2008 were prodrugs.[15] Cytochromes P450 represent one of the dominant classes of enzymes capable of transforming prodrugs into active drugs.[16] However, there are numerous complications that arise from interactions between

Received: April 15, 2011
Revised: September 13, 2011
Published: September 14, 2011

P450-activated prodrugs and other drugs metabolized by P450 enzymes.[17−19] The mARC enzymes are particularly significant for human health because previous studies have shown their ability to reduce *N*-hydroxylated prodrugs, and this bioactivation is not dependent on cytochrome P450 enzymes.[8]

Although mARC enzymes can act on various substrates, the physiological substrate, and thus the physiological function of mARC, still remains enigmatic. On the basis of the high abundance of mARC in liver and kidney,[10] it is tempting to speculate that the function of this enzyme involves detoxification. Yet a most recent study by Clement and coworkers has shown that mARC enzymes may also be involved in the regulation of NO formation as they compete with NO synthase by catalyzing the N-reduction of the NO intermediate *N*-hydroxy-L-arginine.[20] Because of this gap of knowledge, fundamental biophysical and chemical characterization of mARC is crucial for understanding the physiological role and elucidating the mechanistic aspects of N-reduction.

In mammals, there are two isoforms of mARC enzymes, mARC-1 and mARC-2, both having been identified in the inner mitochondrial membrane (referred to as MOSC1 and MOSC2[21]), but only the mARC-2 protein having been shown also to reside in the outer mitochondrial membrane[7] and in peroxisomes.[22,23] A recent successful expression and purification of recombinant human mARC (hmARC) proteins enabled detailed biochemical characterization of both isoforms.[10] Both hmARC-1 and hmARC-2 are 35 kDa proteins sharing a significant degree of sequence similarity, substrate specificity, and biochemical properties, thus not allowing a functional discrimination between mARC-1 and mARC-2 isoforms to be made to date.

An elaborate biochemical analysis of these mARC proteins has shown that a Moco represents their catalytic active center, although the exact chemical structure of the specific Moco was not completely elucidated. On the basis of previous biochemical, mutational, and continuous wave (CW) electron paramagnetic resonance (EPR) evidence, two possibilities for the Mo coordination sphere were suggested.[10] One possibility involves a trioxo species, (MPT)$Mo^{VI}O_3$, which protonates upon reduction to (MPT)$Mo^{V}O_2$(OH) (Scheme 1A). The other possibility is an (MPT)$Mo^{VI}O_2X$ species, with X being either an inorganic or, alternatively, a protein-derived ligand. This latter species also protonates upon reduction, forming (MPT)Mo^{V}O(OH)X (Scheme 1B).[10]

Scheme 1. Proposed Mo(V) Active Site Structures for mARC: (A) (MPT)$Mo^{V}O_2$(OH) and (B) (MPT)Mo^{V}OX(OH) Species, with X Being Either an Inorganic Ligand or a Protein-Derived Ligand[a]

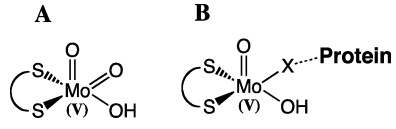

[a]The pyranopterin ligand is shown as ($^{S}_{S}$.

Although the resting state of mARC is Mo(VI), the enzyme(s) can be reduced to a paramagnetic Mo(V) state.[10] This opens up the possibility for detailed investigation of the Mo(V) active center of mARC by CW and high-resolution pulsed EPR techniques. The extensive EPR studies of other molybdoenzymes[24−27] have brought a wealth of information about the nature and structure of the molybdenum ligands as a function of the organism, mutation, and experimental conditions, such as pH or presence of inhibiting anions. One can expect similar biochemically significant structural information to result from EPR studies of mARC. In this work, we use pulsed EPR spectroscopy and theoretical quantum-chemical calculations to address the unresolved problem of the nature of the ligands in the Moco of mARC-2, which has been chosen as subject of this study because it appears to represent the more abundant and important mARC protein in mammals.[22,23] In particular, electron spin echo envelope modulation (ESEEM) spectroscopy is used to obtain direct proof of the nature of the exchangeable ligand in the Mo(V) state and the presence of an oxo ligand(s). Density functional theoretical (DFT) calculations are then used to find out if either of the two proposed structures for the Mo active site of mARC is in agreement with the experimental EPR data.

MATERIALS AND METHODS

Preparation of Human mARC-2 Protein. Recombinant human mARC-2, cyt b_5, and cyt b_5R proteins were expressed and purified as described earlier by Wahl et al.[10]

EPR Sample Preparation. The samples of mARC-2 used for EPR were prepared using buffers of 50 mM phosphate at pH 7.0 containing 300 mM NaCl and 10% glycerol. Enzyme samples (500−800 μM) were mixed with cyt b_5 (5−8 μM) and cyt b_5R (5−8 μM) and made anaerobic at 4 °C. After adding one electron equivalent of degassed solution of 5 mM NADH, the samples were transferred to the EPR tubes flushed with argon and immediately frozen in liquid nitrogen. The D_2O exchange was achieved by concentrating mARC samples to reduce the amount of H_2O and then diluting the samples 30-fold (by volume) with the appropriate buffer in D_2O. The cyt b_5, cyt b_5R, and NADH prepared in D_2O were added, and the sample was transferred to an EPR tube and frozen immediately. The samples in $H_2{}^{17}O$-enriched water were prepared by first concentrating a 60 μL solution of the enzyme in phosphate buffer at pH 8.5 to reduce the amount of $H_2{}^{16}O$. Then, a solution of 50 mM phosphate buffer containing 300 mM NaCl and 10% glycerol was vacuum centrifuged to evaporate the H_2O, and the pelleted buffer was redissolved in the same volume of $H_2{}^{17}O$. Next, mARC, cyt b_5, and cyt b_5R were incubated in 45 μL of $H_2{}^{17}O$ buffer for 30 min−3 h. Finally, the sample was reduced with NADH and immediately frozen in liquid nitrogen. We have to note that the cyt b_5, cyt b_5R, and NADH components were initially in $H_2{}^{16}O$ solution, which resulted in a relatively poor $H_2{}^{17}O$ enrichment of the resulting mARC samples. As a result, our current ^{17}O ESEEM investigation was limited in scope, and we only estimated the *hfi*, but not the *nqi*, for the oxo-^{17}O ligand.

EPR Experiments. The continuous wave (CW) EPR experiments were performed on an X-band EPR spectrometer ESP-300 (Bruker) at a temperature of 77 K. The pulsed EPR experiments were performed on a home-built broadband K_a-band pulsed spectrometer[28] at a temperature of 21 K. The detailed experimental conditions are shown in the figure legends.

DFT Calculations. The DFT calculations were performed using the ORCA computational package (version 2.7.0)[29] and the same methods we have previously reported.[30,31] For geometry optimizations, the BP86 functional[32,33] was employed in conjunction with the all-electron TZVP basis[34,35] in its scalar relativistic recontraction.[36] The protein environment was

modeled through dielectric continuum methods (conductor like screening model, COSMO)[37] using a dielectric constant of four.[38] Density fitting[39−42] was used to accelerate these calculations. Relativistic effects were treated at the level of the zeroth-order regular approximation (ZORA)[43] in one-component form using the model potential of van Wüllen[44] (as implemented in ORCA). The one-center ZORA scalar relativistic correction was also employed.[45] Principal *g*-values and the ^{17}O and ^{1}H *hfi* parameters were calculated using the B3LYP functional,[46,47] the TZVP basis set, the ZORA method, and COSMO (using a dielectric constant of four). Since the scalar relativistic TZVP basis set is less heavily contracted than its nonrelativistic counterpart, further decontraction is not necessary in order to obtain accurate *hfi* and *nqi* predictions close to the basis set limit. The starting coordinates for the different structural models were all derived by truncation and modification of the X-ray crystal structure of *wt* cSO (pdb 1SOX).[48] In each model, the equatorial oxo ligand of 1SOX was replaced with hydroxo, the pterin portion of the molybdopterin cofactor was omitted, and hydrogen atoms were then added where appropriate. For the dioxo/hydroxo model (Scheme 1A), the Mo-coordinated Cys residue of 1SOX was replaced by an oxo ligand at the coordinates of the Cys sulfur prior to optimization. The DFT calculations for Scheme 1B models represented the coordinated protein residue by appropriate organic fragments, i.e., methyl thiolate for Cys. The Ser model was prepared by replacing the 1SOX Cys sulfur atom with an oxygen atom at the same crystallographic coordinates prior to optimization. To simplify the process of rotating the Ser residue (vide infra), Ser was truncated to methoxy. (Having the Ser α carbon would introduce additional geometric degrees of freedom that would greatly complicate the optimization process while not influencing the calculated spectroscopic trends.) In a similar way, the Met model was prepared using dimethyl sulfide with the sulfur atom placed at the 1SOX Cys sulfur coordinates prior to optimization. Twelve structural models were obtained for the dioxo/hydroxo model (Scheme 1A) by rotating the hydroxo ligand in fixed 30° increments about the Mo(V)−OH bond (with respect to the Mo(V) oxo bond) and optimizing with all other parameters relaxed. For the Cys, Ser, and Met models (Scheme 1B), the same hydroxo ligand rotation was carried out along with simultaneous rotation of the "Cys", "Ser", or "Met" ligands in 60° increments (where the methyl coincident to the axial oxo was defined as 0°); 72 additional structural models were obtained for each. The Cartesian coordinates of all optimized models (in *XYZ*-file format) for which all of the property calculations were performed are included in the Supporting Information.

RESULTS AND DISCUSSION

1. CW EPR and Pulsed EPR Field Sweeps. Trace 1 in Figure 1 shows the CW EPR spectrum of the Mo(V) center of mARC-2 prepared at pH 7.0 in H_2O buffer. The spectrum of a sample prepared at pH 8.5 was identical. This spectrum is described by a nearly axial **g**-tensor with $g_{\|} \approx 2.000$ and $g_{\perp} \approx 1.965$ (similar to the numbers estimated earlier $(g_Z, g_Y, g_X) = (1.9994, 1.9658, 1.9616)$[10] and shows well-resolved doublet splittings at the turning points: about 1 mT at $g_{\|}$ and 1.6 mT at $g_{\perp}$. The EPR spectrum of the sample prepared in D_2O (trace 2 in Figure 1) does not show the splittings, which proves that they originate from a hyperfine interaction (*hfi*) with an exchangeable proton. This proton most likely belongs to an OH ligand. The *hfi* constant of 30−45 MHz (recalculated from the splittings in mT) indicates that the OH bond of this putative OH ligand is nearly in the plane of the Mo(V) d_{xy} orbital carrying the unpaired electron.

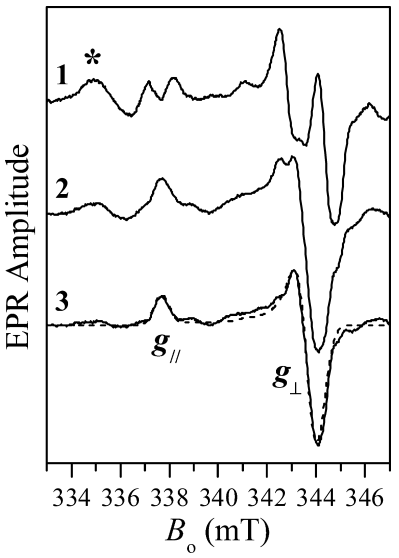

Figure 1. CW EPR spectra of mARC-2 in the Mo(V) state. Trace 1, the sample in H_2O; trace 2, the sample in 65% D_2O (see text); solid trace 3, the sample in pure D_2O (obtained as a difference between trace 2 and appropriately normalized trace 1); dashed trace 3, simulated with $g_{\|} = 2.000$ and $g_{\perp} = 1.965$. Experimental conditions: $\nu_{mw} = 9.453$ GHz; mw power, 2 mW; modulation amplitude, 0.2 mT; temperature, 77 K. The asterisk marks the signal of unknown origin that is always observed in mARC enzymes.

Apart from the major Mo(V) signal described above, there is an additional minor signal present at $g \sim 2.01$ (marked by an asterisk in Figure 1). This signal is present regardless of the presence of the Mo(V) signal. The origin of this signal is not known, and it was not investigated further in this work.

2. ^{2}H ESEEM in the Samples in D_2O Buffer. The purpose of spectroscopic investigation of mARC-2 in D_2O buffer is twofold. First, ^{2}H has spin $I = 1$ and a nonzero nuclear quadrupole interaction (*nqi*). The quadrupole coupling constant of ^{2}H can help independently identify the exchangeable ligand containing this deuteron. Second, the dramatically smaller magnetic moment of ^{2}H compared with ^{1}H makes it readily accessible for a productive ESEEM examination in order to obtain a good estimate of the *hfi* tensor components and the orientation of the *hfi* tensor with respect to the principal axes system of the **g**-tensor (*g*-frame).

Because of the relatively strong *hfi*, the ESEEM measurements were performed at the mw K_a band. This has allowed us to organize the weak *hfi* regime for the ligand deuteron ($\nu_D > A/2$, where ν_D is the deuteron Zeeman frequency and A is the diagonal part of the *hfi* constant) and to ensure that the *nqi* splittings, $\Delta\nu_{Q}$, of the fundamental lines were much smaller than the fundamental frequencies ($\Delta\nu_Q \ll \nu_{\alpha,\beta} \approx \nu_D \pm A/2$). As an example, Figure 2a shows a hyperfine sublevel correlation (HYSCORE) spectrum of the sample in D_2O obtained at $g_{\perp}$. The correlation features (ν_α, ν_β) and (ν_β, ν_α) due to the neighboring ^{2}H are located at about (4, 10) and (10, 4) MHz, symmetrically with respect to $\nu_D \approx 7.1$ MHz. The splitting between these correlation features is determined by the *hfi*. Each of these features forms a pattern of approximately antidiagonal ridges, the splitting between which (measured along the main diagonal) is determined by the *nqi*. The detailed

dx.doi.org/10.1021/bi2005762 | *Biochemistry* 2011, 50, 8813−8822

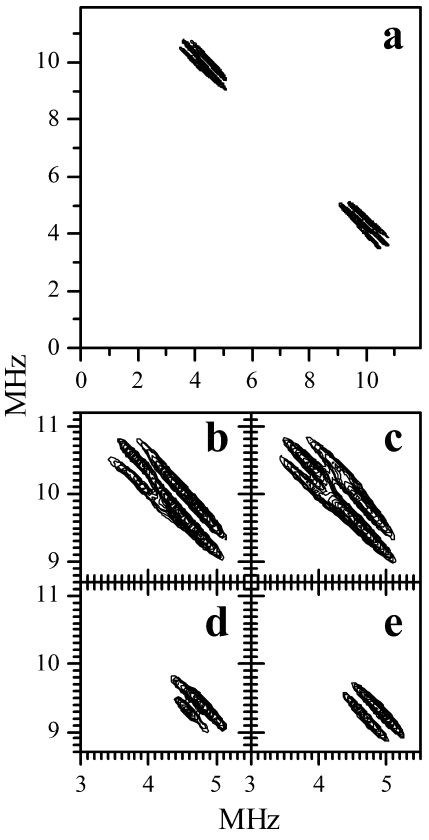

Figure 2. HYSCORE spectra of the Mo(V) center of mARC-2 in D_2O. Panel a shows the experimental spectrum at $g_\perp$ (B_0 = 1086.2 mT). Panels b and d show an expanded view of one of the correlation features observed in the experimental spectra at $g_\perp$ and $g_\parallel$ (B_0 = 1068.6 mT), respectively. Experimental conditions: ν_{mw} = 29.858 GHz; interval between the first and second mw pulses, τ = 150 ns; durations of mw pulses, 10, 10, 17, 10 ns; temperature, 21 K. Panels c and e show the simulated spectra for a deuteron with a_D = 5 MHz, $T_\perp$ = −1.3 MHz, e^2Qq/h = 0.22 MHz, η = 0. The orientation of the $T_\parallel$ axis with respect to the *g*-frame (defined by (g_X, g_Y, g_Z) = (1.965, 1.965, 2.000)) is given by the polar and azimuthal angles θ_h = 75° and φ_h = 30°. The isotropic *hfi* was Gaussian-distributed with the width of Δa_D = 1 MHz. The orientation of the *nqi* axis is given by θ_q = 80° and φ_q = 0°. The accuracy of determination of all of the angles is ±5°.

nqi structure of the correlation features observed at $g_\perp$ and $g_\parallel$ is shown in panels b and d of Figure 2.

The minimal hyperfine splitting between the HYSCORE lines is observed at $g_\parallel$ ($A_\parallel \sim 4$ MHz, see Figure 2d), and the largest one is observed at $g_\perp$ ($A_\perp \sim 7.5$ MHz, see Figure 2a or 2b). For the intermediate EPR positions from $g_\parallel$ toward $g_\perp$ the maximal *hfi* splitting monotonously increases, as does the length of the ridges, which indicates that the *hfi* tensor has a large variation in the *XY* plane of the *g*-frame (corresponds to $g_\perp$). For example, if the *hfi* tensor is nearly axial, then its axis is at a large angle with the *g*-frame *Z*-axis (corresponds to $g_\parallel$). From these considerations, the *hfi* parameters can be estimated as a_D = 5.2 MHz and $T_\perp$ = −1.2 MHz, where a_D is the isotropic *hfi* constant and $T_\perp$ is the perpendicular component of the anisotropic *hfi* tensor. As a starting approximation for the polar angle θ_h between the *hfi* axis and the axis of $g_\parallel$ (*Z*) one can take θ_h = 90°.

While in principle the ^{2}H *nqi* can be determined from the splittings of the sum combination line (obtained with high resolution in τ-integrated four-pulse ESEEM spectra[49]), in the given system the sum combination feature is contributed to by both the matrix deuterons and the nearby OD ligand deuteron. The matrix line is suppressed in HYSCORE spectra at τ = 150 ns (see, e.g., Figure 2a), but it is seen at other τ values, as well as in two-pulse ESEEM spectra (see Supporting Information). Therefore, the information about the *nqi* was obtained directly from the HYSCORE spectra.

The maximum splitting between the antidiagonal ridges of the HYSCORE lines is observed at $g_\perp$ ($\Delta\nu_Q \sim 0.35$ MHz, see Figure 2b), and it correlates with the maximum *hfi* splitting (i.e., it is observed at the outer edges of the HYSCORE features). This indicates that the main *nqi* axis is close to the *XY* plane of the *g*-frame and that the angle between the main *hfi* and *nqi* axes is not very large (significantly smaller than 55°). Since hydrogen is attached to a neighboring atom (e.g., oxygen) with a single covalent bond, the *nqi* tensor is approximately axial, although the off-axis hydrogen bonding may introduce some rhombicity.[50] For the axial *nqi* tensor the quadrupole splitting of the fundamental frequencies is equal to (to first order)

$$\Delta\nu_Q = \frac{3}{4}\frac{e^2Qq}{h}(3\cos^2\theta_{qB} - 1) \quad (1)$$

where e^2Qq/h is the quadrupole coupling constant and θ_{qB} is the angle between the *nqi* tensor axis and the magnetic field, $\mathbf{B}_0$. The maximal $\Delta\nu_Q$ of 0.35 MHz observed in HYSCORE spectra obviously corresponds to θ_{qB} = 0°, which results in $e^2Qq/h = (2/3)\Delta\nu_Q \approx 0.23$ MHz.

The *hfi* and *nqi* parameters estimated above were used as a starting approximation in numerical calculations of the ^{2}H HYSCORE spectra. In these simulations the anisotropic *hfi* and *nqi* tensors were assumed to be axial. The simulations have resulted in the following set of parameters: a_D = 5 MHz, $T_\perp$ = −1.3 MHz, e^2Qq/h = 0.22 MHz, η = 0. The orientation of the $T_\parallel$ axis with respect to the *g*-frame is defined by the polar and azimuthal angles θ_h = 75° and φ_h = 30°. The isotropic *hfi* was Gaussian-distributed with the width of Δa_D = 1 MHz. The orientation of the *nqi* axis is defined by θ_q = 80° and φ_q = 0°. The accuracy of determination of all of the angles is ±5°. With regard to the azimuthal angles one has to note that for the axial *g*-frame only the difference $|\varphi_h - \varphi_q| \sim 30°$ is meaningful, while the separate absolute values of φ_h and φ_q are meaningless. The spectra simulated for $g_\perp$ and $g_\parallel$ positions are shown in Figures 2c and 2e, respectively.

3. ^{17}O ESEEM in the Samples on $H_2{}^{17}O$ Buffer. The experiments on the samples prepared in $H_2{}^{17}O$ buffer were performed in order to shed light on the possible presence of an exchangeable axial oxo ligand. The ^{17}O isotope (natural abundance 0.038%) has nuclear spin I = 5/2, which makes it observable by magnetic resonance spectroscopic methods after appropriate enrichment. On the basis of our experience with the Mo(V) center of SO[30] and the oxo exchange results for model Mo complexes,[51] we expected that the $^{16}O \leftrightarrow {}^{17}O$ exchange for the oxo ligand will be slow (tens of minutes), and the yield of ^{17}O-enriched Mo center will depend on the incubation time in the ^{17}O-enriched buffer. The observation of such a slowly exchanging oxygen would indicate the presence of the oxo ligand.

Figure 3 shows primary ESEEM spectra of mARC-2 incubated in $H_2{}^{17}O$-enriched buffer (80−84.9%) for 3 h (solid trace, "long incubation") and 30 min (dashed trace, "short incubation"). The low-frequency lines originate from

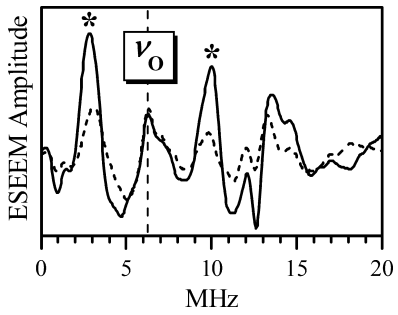

Figure 3. Primary ESEEM spectra of the Mo(V) center of mARC-2 in $H_2{}^{17}O$-enriched buffer at pH 8.5. Solid and dashed traces correspond to the long-incubation (3 h) and short-incubation (30 min) samples, respectively. The asterisks mark the ^{17}O lines from the oxo ligand. Vertical dashed line indicates the position of the ^{17}O Zeeman frequency, ν_O. Experimental conditions: ν_{mw} = 29.794 GHz; magnetic field, B_0 = 1084 mT ($g_\perp$); mw pulses, 10 and 15 ns; temperature, 21 K.

^{17}O, since the natural abundance sample does not show any low-frequency lines. The two prominent features at about 2.9 and 9.8 MHz marked by asterisks are significantly smaller in the spectrum of the short-incubation sample than in the spectrum of the long-incubation sample. The 2.9 and 9.8 MHz lines are located symmetrically with respect to the Zeeman frequency of ^{17}O ($\nu_O \approx 6.3$ MHz), and they represent the ν_α and ν_β fundamental features, each of which is contributed by five $\Delta m_I = 1$ transitions. All of these transitions except the $|-1/2\rangle \leftrightarrow |1/2\rangle$ one are somewhat broadened by the *nqi*, and the observable lines are therefore dominated by the $|-1/2\rangle \leftrightarrow |1/2\rangle$ transition which does not depend on *nqi* to first order.[52,53]

From the lines observed in the spectrum of the long-incubation sample in Figure 3 the ^{17}O *hfi* constant corresponding to $g_\perp$, $A_\perp \approx 6.9$ MHz can thus be evaluated. The ^{17}O *hfi* constant (measured as a splitting between these two lines) monotonously decreases toward $g_\parallel$, where it becomes equal to $A_\parallel \approx 3.8$ MHz. Figure 4 shows the

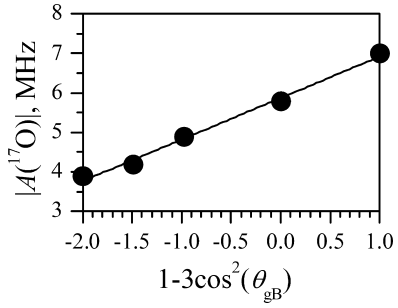

Figure 4. Dependence of the *hfi* constant of oxo-^{17}O, A, on EPR position. The EPR position is expressed in terms of $1 - 3\cos^2(\theta_{gB})$, where θ_{gB} is the angle between the axis of $g_\parallel$ and the direction of $\mathbf{B}_0$. Filled circles, experimental *hfi* constant. Solid line, least-squares fit by the function $A = a_{iso} + T_\perp(1 - 3\cos^2(\theta_{gB}))$, where a_{iso} is the isotropic *hfi* constant and $T_\perp$ is the perpendicular component of the axial anisotropic *hfi* tensor. The resulting fitting parameters are $a_{iso} = \pm 5.9$ MHz and $T_\perp = \pm 1.05$ MHz (both positive or both negative).

dependence of the *hfi* constant of this exchangeable ^{17}O as a function of $1 - 3\cos^2(\theta_{gB})$, where θ_{gB} is the angle between the axis of $g_\parallel$ and the direction of $\mathbf{B}_0$. This dependence is linear with good accuracy, which indicates that the long axis of the anisotropic *hfi* tensor is about parallel to the axis of $g_\parallel$. Assuming an axial *hfi* tensor, we can estimate $a_O = \pm 5.9$ MHz and $T_\perp = \pm 1.05$ MHz (both positive or both negative) from a linear least-squares fit of the experimental data shown in Figure 4.

These *hfi* parameters are similar to those obtained for the oxo ^{17}O ligand in a model Mo(V) complex $[Mo(V)^{17}O(SPh)_4]^-$ (a_O = 6.5 MHz and $T_\perp$ = 1.6 MHz[52]) and in the Mo(V) center of the high-pH (*hpH*) form of SO (a_O = 6.3 MHz, (T_{11}, T_{22}, T_{33}) = (−2.4, −1.3, 4) MHz[30]). In addition, the amplitude of the observed ^{17}O lines in the ESEEM spectra of the long-incubation sample was much greater than for the short-incubation sample. These observations indicate that the observed ^{17}O lines belong to an exchangeable oxo ligand.

It is interesting to note that the *hfi* of the oxo ligand in the Mo(V) complexes is noticeably weaker than in the oxovanadium *aquo* complex (a_{iso} = 8.4 MHz and $T_\perp$ = 7.6 MHz),[54] although the orientation dependence of the *hfi* parameters[52,54] and the characteristic property of very slow exchange rate of this oxygen with the buffer[30,51] are common for both species.

In our ^{17}O ESEEM experiments we did not observe the features attributable to the equatorial ^{17}OH ligand. Our experience with the Mo(V) center of SO shows, however, that because of relatively strong *hfi* (may reach tens of megahertz), the observation of the equatorial oxygen is difficult even for the samples with very strong Mo(V) EPR signals.[28,30,31,55] The Mo(V) EPR signals of mARC-2 were significantly smaller than those we typically obtained for SO. In addition, the ^{17}O enrichment was lower because cyt b_5, cyt b_5R, and NADH were in $H_2{}^{16}O$ buffer (see Materials and Methods). Therefore, the lack of observation of the equatorial ^{17}O ligand is not surprising.

4. DFT Calculations To Address the Nature of the Unknown Ligand. As a result of our experiments, we have established that the Mo(V) center of mARC-2 enzyme has an exchangeable equatorial OH ligand and an exchangeable axial oxo ligand. As shown in earlier work,[10] two of the equatorial ligands are provided by the pyranopterindithiolate (MPT) moiety, which represents a common ligand among all known molybdenum centers in various enzymes. The nature of the one remaining equatorial ligand is currently unclear. In Scheme 1B the remaining equatorial ligand, X, is an inorganic or a protein-derived ligand. Our current pulsed EPR results exclude nitrogen coordination by such amino acids as histidine, tryptophan, and lysine because no nitrogen ESEEM or EPR splittings are observed. There are several possibilities for EPR-silent protein-derived ligands that coordinate to Mo(V) through nonmagnetic nuclei such as sulfur (cysteine and methionine) and oxygen (serine, tyrosine, or carboxylate). Another structural possibility mentioned in the previous work[10] is a dioxo species (MPT)Mo^VO_2(OH) (Scheme 1A), which is not coordinated to the protein.

While obviously additional experimental work is needed to definitively pinpoint the undetermined equatorial ligand, we performed here an analysis of the dioxo and protein-coordinated species (Scheme 1) using DFT calculations. The purposes of this analysis were (1) to determine if the dioxo species is in agreement with the EPR experimental data obtained previously[10] and in this work and (2) to find out if the spectroscopic parameters calculated for various protein-derived ligands are sufficiently different to permit a specific assignment of the ligand based on comparison with the experimental data. The details of the calculations are described in Materials and Methods.

On the basis of our experience with DFT calculations for oxomolybdenum model compounds[52] and for the Mo(V) center of SO under various conditions,[26,30,31] we will approximate the expected possible deviation of the calculated *hfi* parameters from the true ones as the larger of ±20% or ±3 MHz. The situation with the **g**-tensor calculations is more complicated. Previous work has demonstrated that reasonable agreement between calculated and experimental *g*-values can be obtained for well-defined chemical structures.[56−60] In this work, however, the calculated **g**-tensor components of the protein-bound Moco showed erratic dependence on the orientations of the equatorial hydroxo and the protein-derived ligands, in stark contrast to the *hfi* parameters, which show an oscillatory behavior (see Supporting Information). A possible reason for this outcome could be our use of structural constraints, resulting in relatively high energies for some of the structures. The overall range of calculated principal *g*-values (from ∼1.6 to ∼2.2) significantly exceeds the *g*-anisotropy observed experimentally (from ∼1.96 to ∼2.0). The combination of these two factors (large range and erratic behavior) prevents reliable structural conclusions based on *g*-values.

4a. DFT Calculations for (MPT)Mo^{V}O$_2$(OH). Let us consider first the dioxo species, (MPT)Mo^{V}O$_2$(OH) (Scheme 1A). This structure contains only one variable parameter, namely, the orientation of the OH ligand. Therefore, we performed the DFT calculations for various orientations of this ligand. The OH orientation was described by the dihedral angle θ_{OH} between the O═Mo−O(H) and (O═)Mo−OH planes. For each (constrained) θ_{OH} the rest of the complex geometry was optimized, and the spectroscopic parameters were calculated.

Figure 5a shows the calculated dependence of the isotropic *hfi* constant of the OH ligand proton, a_H, as a function of θ_{OH}. This function shows an oscillation with a period of about 180°, with maxima at $\theta_{OH} \approx 120°$ and 300° and minima at $\theta_{OH} \approx 40°$ and 200°. The experimental $a_H \approx 32.5$ MHz (as recalculated from a_D determined in this work) is shown by a horizontal gray strip in Figure 5a. The range of angles θ_{OH}, for which the calculated and experimental a_H are in a qualitative agreement, is approximately between 270° and 330°. The vertical gray strip crossing Figure 5 highlights this range of θ_{OH}.

The calculated isotropic *hfi* constants of the ^{17}O oxo ligands are shown in Figure 5b. The horizontal gray strip in this panel shows the experimental $a_O = -5.9$ MHz determined using ESEEM in this work. The calculated a_O for both of the oxo ligands are simultaneously in agreement with the experimental $a_O = -5.9$ MHz at several values of θ_{OH}, in particular, at $\theta_{OH} \sim 290°-310°$, which also provides the agreement between the calculated and experimental a_H. The possible positive *hfi* constant, $a_O = 5.9$ MHz, is in disagreement with the calculation.

Figure 5c shows the long component of the anisotropic *hfi* tensor, $T_{||}$, of the oxo ^{17}O ligands. For $\theta_{OH} \sim 300°$, the calculated values of $T_{||}$ range from −20 to −35 MHz and are in stark disagreement with the experimental $T_{||} = -2T_{\perp} = 2.1$ MHz, both in sign and in magnitude. Thus, the comparisons of the calculated and experimental spectroscopic parameters shown in Figure 5 allows us to conclude that the dioxo Mo(V) complex of Scheme 1A is not an appropriate model for the Moco in mARC-2 enzyme.

A somewhat unusual feature of the electronic structure of the double-oxo complex is that the two oxo ligands provide approximately equal contributions to the overall crystal field at Mo(V). This results in the natural *z*-axis for the real d-orbital set being oriented between the oxo ligands. Accordingly, the d_{xy} orbital (singly occupied molecular orbital, SOMO) plane is also tilted by about 30°−40° from the orientation expected for a single (axial) oxo ligand. This tilt of the d_{xy} orbital results in the shift of the a_H dependence on θ_{OH} and in the possibility of direct π-overlap between the p-orbitals of the oxo ligands with the SOMO, which results in unusually strong isotropic and anisotropic *hfi* constants.

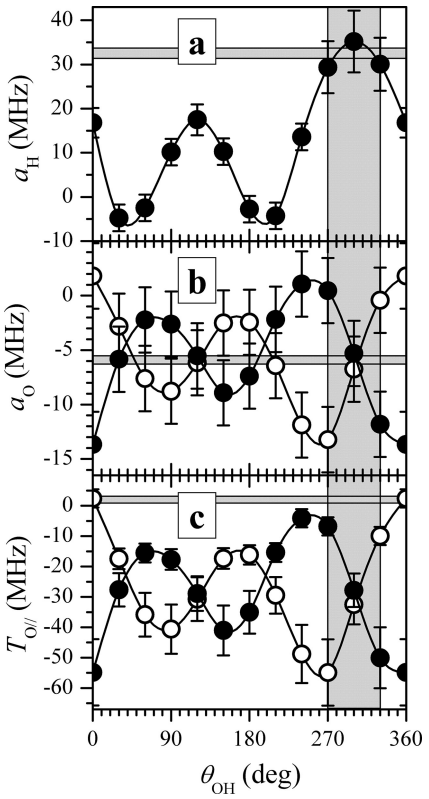

Figure 5. Results of DFT calculations for (MPT)Mo^{V}O$_2$(OH) as a function of θ_{OH}. Panel a shows the isotropic *hfi* constant of the hydroxyl ligand proton, a_H, panel b shows the isotropic *hfi* constants of the oxo ligands, a_O, and panel c shows the long components of the anisotropic *hfi* tensors of the oxo ligands, $T_{O||}$. The filled and open circles in panels b and c correspond to the axial and equatorial oxo ligands, respectively. Gray horizontal strips show the experimental values of the corresponding parameters. The vertical gray strip crossing all panels shows the range of angles θ_{OH} providing an agreement between the experimental and calculated a_H. The vertical lines through each point in the panels indicate the estimated possible deviations of the calculated parameters from the true ones.

4b. DFT Calculations for (MPT)Mo^{V}O(OH)X. In this section we consider the (MPT)Mo^{V}O(OH)X model (Scheme 1B) with X = Ser, Met, or Cys. Detailed explanation is given for X = Ser as an example of a protein-derived oxygen ligand. This type of Moco has two degrees of freedom: the orientation of the OH ligand and the orientation of the serine ligand. The OH ligand orientation was described using θ_{OH} defined similar to that in the dioxo model considered above. The serine orientation was defined in similar way, with θ_{Ser} being a dihedral angle between the O═Mo−O(C$_{Ser}$) and (O═)Mo−OC$_{Ser}$ planes. For each (constrained) θ_{OH} and θ_{Ser} the rest of the complex geometry was optimized, and the spectroscopic parameters were calculated. The angles θ_{OH} and θ_{Ser} were varied with steps of 30° and 60°, respectively, and the data were presented as graphs against θ_{OH}, with θ_{Ser} being a parameter. Because of the large total number of the plots, it was not reasonable to present

all of them in the article. We have presented therefore only the data that were immediately relevant to the current discussion.

Figure 6a shows the dependences of a_H on θ_{OH} for various values of θ_{Ser}. One can see that all of the plots are very similar,

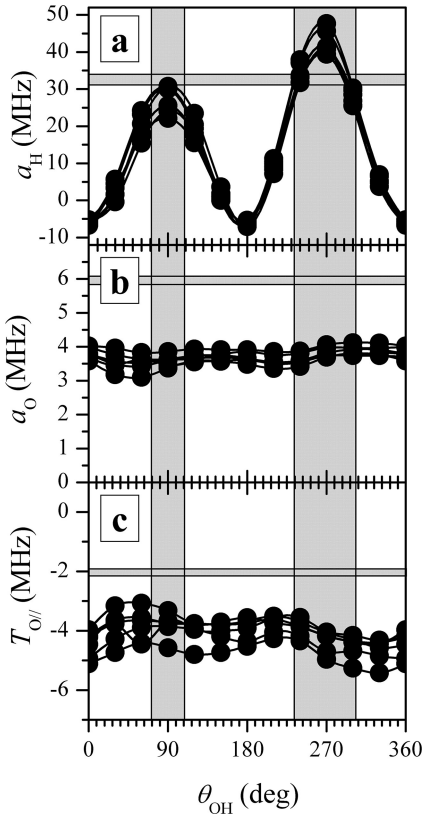

Figure 6. Results of DFT calculations for (MPT)Mo^{V}O(OH)Ser as a function of θ_{OH} and θ_{Ser}. The general structure of Figure 6 is similar to that of Figure 5. The plots for different θ_{Ser} values (from 0° to 300°, with the step of 60°) are overlaid to show the range of variation of the calculated parameters as a function of θ_{Ser}. The filled circles in panels b and c correspond to the axial oxo group. Gray horizontal strips show the experimental values of the corresponding parameters. Vertical gray strips crossing all panels show the range of angles θ_{OH} providing an agreement between the experimental and calculated a_H.

with a_H being an oscillating function of θ_{OH}, with minima at θ_{OH} = 0° and 180° and maxima at θ_{OH} = 90° and 270°. The maximal values of a_H somewhat depend on θ_{Ser} and reach 40–50 MHz. Figures 6b and 6c show similar plots for a_O and the larger anisotropic *hfi* component of the oxo ligand. Unlike a_H, the oxo-^{17}O *hfi* parameters show very little dependence on the orientations of the hydroxo and serine ligands. Figure 6 does not show the estimated possible deviations of the calculated values from the true ones in order to avoid overcrowding the figure. However, the estimated deviations in the calculated ^{1}H and ^{17}O *hfi* parameters are similar to those presented in Figure 5. Thus, within the limitations of the DFT calculations of the ^{1}H and ^{17}O *hfi* parameters, the model with coordinated serine cannot be excluded from consideration as representing the Moco of the mARC-2 enzyme.

If serine is assumed to be the fourth equatorial ligand, then the immediate ligand environment of the Mo(V) center is the same as that in the human SO (hSO), where the cysteine residue coordinated to the Mo center was mutated to serine.[61] In this C207S mutant hSO, the Mo(VI) state was shown to have three oxo ligands, but one of the equatorial oxo ligands became replaced by a serine ligand in the Mo(V) state, while the other one became replaced by a hydroxyl.[61] The Mo(V) EPR spectrum of C207S hSO was extremely rhombic, with (g_X, g_Y, g_Z) = (1.9545, 1.9654, 1.9789). The *hfi* with the proton of the equatorial OH ligand resulted in a resolved splitting at the intermediate turning point, and the EPR spectrum was successfully simulated assuming the ^{1}H *hfi* tensor ($|A_X|$, $|A_Y|$, $|A_Z|$) ≈ (6, 12, 6) MHz. Assuming an axial *hfi* tensor with $A_X = A_Z$, one either obtains (a_H, $T_\perp$) ≈ (8, −2) MHz or (a_H, $T_\perp$) ≈ (0, −6) MHz, depending on the choice of signs of A_X and A_Z. The magnitude of $T_\perp$ in the second set is much more reasonable than in the first one, and it is comparable with $T_\perp$ known for the OH ligand proton in SO[62,63] and DMSOR.[64] Therefore, we consider the second set to be the correct one. The corresponding value of a_H (∼0 MHz) is also presented in Table 1.

It is thus clear that the EPR parameters of the Mo(V) species of mARC-2 and C207S hSO are quite different from one another. These parameters are summarized in Table 1, together with the corresponding parameters of low-pH (*lpH*) and *hpH* SO used in the following discussion.

From Figure 6a it is obvious that the difference in a_H between C207S hSO and mARC-2 can be explained by different θ_{OH} (near 0° or 180° vs near 90° or 270°). The similar structural change explains the difference in a_H between *hpH* and *lpH* SO (∼0 and ∼26 MHz, respectively).[62,63] In SO, the reorientation of the OH ligand is accompanied by an increase in the rhombicity of the **g**-tensor, $|g_X - g_Y|/|g_X - g_Z|$, from ∼0.2 in *lpH* SO to ∼0.24 in *hpH* SO. An increase of **g**-tensor rhombicity (from ≤0.1 to ∼0.42) is also evident from comparison of mARC-2 and C207S hSO (see Table 1). Therefore, the assumption of the fourth equatorial ligand in mARC-2 being a serine residue does not contradict any of the available EPR data. This, however, does not necessarily mean that Ser *is* the ligand. In fact, the DFT calculations for Met and Cys (see Supporting Information) resulted in ^{1}H and ^{17}O *hfi* parameters similar to those obtained for Ser, and all of the experimental EPR data for mARC-2 are generally similar to those obtained earlier for SO.[24,27] Therefore, it is unlikely that DFT calculations can distinguish between various possible Mo(V) centers with the general structures (MPT)Mo^{V}O-

Table 1. Principal *g*-Values and Isotropic *hfi* Constants of the OH Ligand Proton for Mo(V) Centers of SO and mARC-2 Enzymes

Moco	g_Z	g_Y	g_X	a_H (MHz)	ref
lpH SO	2.004	1.972	1.966	26	*g*: 66; a_H: 63
mARC-2	1.999 (2.000)	1.966 (1.965)	1.962 (1.965)	32	*g*: 10, this work; a_H: this work
hpH SO	1.987	1.964	1.953	0	*g*: 66; a_H: 62
C207S hSO	1.979	1.965	1.955	0	61

dx.doi.org/10.1021/bi2005762|*Biochemistry* 2011, 50, 8813–8822

(OH)−O−... or (MPT)$Mo^{V}O$(OH)−S−..., especially taking into account the unknown orientation of the protein-derived ligand. Further biochemical and structural studies are necessary to identify the fourth ligand in mARC enzymes. Figure S7 of the Supporting Information combines the experimental spectroscopic information about the directions of the *hfi* and *nqi* tensors obtained in this work with the overall conclusion of the DFT calculations about the protein-bound oxomolybdenum center.

CONCLUSION

The ^{1}H and ^{17}O ESEEM investigation of mARC-2 enzyme in this work has provided evidence that the Moco in the Mo(V) state has an equatorial OH ligand and an exchangeable axial oxo ligand. Two of the equatorial ligands were earlier shown to belong to the pterin cofactor. The fourth equatorial ligand cannot be nitrogen and should be EPR-silent (O or S). In order to shed light on the nature of the fourth equatorial ligand, DFT calculations have been performed. The comparison of the experimental and calculated ^{1}H and ^{17}O *hfi* data has established that the (MPT)$Mo^{V}O_2$(OH) (dioxo) model is in disagreement with the experiment. On the other hand, the calculations for the (MPT)Mo^{V}O(OH)X model where X is a protein-derived amino acid residue (Ser, Cys, or Met) have shown that, within the limited accuracy of the experimental results and especially the DFT calculations, any of these residues can be considered in agreement with the experimental data. One potential possibility for identifying the protein-derived equatorial ligand may be electron−nuclear double resonance (ENDOR) detection of second-sphere protons belonging to this ligand,[65] and such studies are underway.

ASSOCIATED CONTENT

Supporting Information

Two-pulse ESEEM spectra of mARC-2 in D_2O; the dependence of the calculated **g**-tensor components of the dioxo, serine-coordinated, Cys-coordinated, and Met-coordinated Moco on the orientations of the equatorial hydroxo and the protein-derived ligands; *hfi* parameters calculated for Cys-coordinated and Met-coordinated Moco model; orientations of the *hfi* and *nqi* tensors of the equatorial hydroxyl ligand deuteron and axial ^{17}O oxo ligand with respect to the mARC-2 Mo(V) *g*-frame; the Cartesian coordinates of DFT-optimized structural models, for which the property calculations were performed. This material is available free of charge via the Internet at http://pubs.acs.org.

AUTHOR INFORMATION

Corresponding Author

*Phone: 520-621-2245. Fax: (520) 626-8065. E-mail: jenemark@email.arizona.edu.

Funding

This research was supported by NIH Grant GM-037773 (to J.H.E.) and DFG (Deutsche Forschungsgemeinschaft) Grant Me1266/24-1 (to R.R.M.). The construction of the pulsed EPR spectrometers was supported by grants from the NSF (DBI-0139459, DBI-9604939, and BIR-9224431) and the NIH (S10RR020959).

ACKNOWLEDGMENTS

We are grateful to Professor Russ Hille and Dimitri Niks from Department of Biochemistry and Molecular Biology, UC Riverside, for helpful discussions on EPR sample preparation.

ABBREVIATIONS

SO, sulfite oxidase; mARC, mitochondrial amidoxime reducing component; Moco, molybdenum cofactor; EPR, electron paramagnetic resonance; CW, continuous wave; DFT, density functional theory; ESEEM, electron spin echo envelope modulation; HYSCORE, hypefine sublevel correlation; *hfi*, hyperfine interaction; *nqi*, nuclear quadrupole interaction.

REFERENCES

(1) Hille, R. (1997) Mechanistic aspects of the mononuclear molybdenum enzymes. *J. Biol. Inorg. Chem 2*, 804−809.

(2) Hille, R. (1996) The mononuclear molybdenum enzymes. *Chem. Rev. 96*, 2757−2816.

(3) Hille, R., Sigel, A., and Sigel, H. (2002) Molybdenum and tungsten. Their roles in biological processes, in *Metal Ions in Biological Systems*, pp 187−227, Marcel Dekker, Inc., New York.

(4) Hille, R. (2002) Molybdenum enzymes containing the pyranopterin cofactor: An overview. *Molybdenum Tungsten 39*, 187−226.

(5) Hille, R. (2005) Molybdenum-containing hydroxylases. *Arch. Biochem. Biophys. 433*, 107−116.

(6) Gruenewald, S., Wahl, B., Bittner, F., Hungeling, H., Kanzow, S., Kotthaus, J., Schwering, U., Mendel, R. R., and Clement, B. (2008) The fourth molybdenum containing enzyme mARC: Cloning and involvement in the activation of N-hydroxylated prodrugs. *J. Med. Chem. 51*, 8173−8177.

(7) Havemeyer, A., Bittner, F., Wollers, S., Mendel, R., Kunze, T., and Clement, B. (2006) Identification of the missing component in the mitochondrial benzamidoxime prodrug-converting system as a novel molybdenum enzyme. *J. Biol. Chem. 281*, 34796−34802.

(8) Havemeyer, A., Grunewald, S., Wahl, B., Bittner, F., Mendel, R., Erdelyi, P., Fischer, J., and Clement, B. (2010) Reduction of *N*-hydroxy-sulfonamides, including *N*-hydroxy-valdecoxib, by the molybdenum-containing enzyme mARC. *Drug Metab. Dispos. 38*, 1917−1921.

(9) Mendel, R. R. (2009) Cell biology of molybdenum. *BioFactors 35*, 429−434.

(10) Wahl, B., Reichmann, D., Niks, D., Krompholz, N., Havemeyer, A., Clement, B., Messerschmidt, T., Rothkegel, M., Biester, H., Hille, R., Mendel, R. R., and Bittner, F. (2010) Biochemical and spectroscopic characterization of the human mitochondrial amidoxime reducing components hmARC-1 and hmARC-2 suggests the existence of a new molybdenum enzyme family in eukaryotes. *J. Biol. Chem. 285*, 37847−37859.

(11) Wollers, S., Heidenreich, T., Zarepour, M., Zachmann, D., Kraft, C., Zhao, Y. D., Mendel, R. R., and Bittner, F. (2008) Binding of sulfurated molybdenum cofactor to the C-terminal domain of aba3 from *Arabidopsis thaliana* provides insight into the mechanism of molybdenum cofactor sulfuration. *J. Biol. Chem. 283*, 9642−9650.

(12) Anantharaman, V., and Aravind, L. (2002) MOSC domains: Ancient, predicted sulfur-carrier domains, present in diverse metal-sulfur cluster biosynthesis proteins including molybdenum cofactor sulfurases. *FEMS Microbiol. Lett. 207*, 55−61.

(13) Ichida, K., Matsumura, T., Sakuma, R., Hosoya, T., and Nishino, T. (2000) Mutation of human molybdenum cofactor sulfurase gene is responsible for classical xanthinuria type II. *Biochem. Biophys. Res. Commun. 282*, 1194−1200.

(14) Watanabe, T., Ihara, N., Itoh, T., Fujita, T., and Sugimoto, Y. (2000) Deletion mutation in *drosophila ma-l* homologous, putative molybdopterin cofactor sulfurase gene is associated with bovine xanthinuria type II. *J. Biol. Chem. 275*, 21789−21792.

(15) Stella, V. J. (2010) Prodrugs: Some thoughts and current issues. *J. Pharm. Sci. 99*, 4755−4764.
(16) Huttunen, K. M., Mahonen, N., Raunio, H., and Rautio, J. (2008) Cytochrome p450-activated prodrugs: Targeted drug delivery. *Curr. Med. Chem. 15*, 2346−2365.
(17) Jeong, S., Nguyen, P. D., and Desta, Z. (2009) Comprehensive in vitro analysis of voriconazole inhibition of eight cytochrome p450 (CYP) enzymes: Major effect on CYPs 2B6, 2C9, 2C19, and 3A. *Antimicrob. Agents Chemother. 53*, 541−551.
(18) Flockhart, D. A. (2009) *Drug interactions: Cytochrome p450 drug interaction table*, Indiana University School of Medicine; http://medicine.iupui.edu/clinpharm/ddis/table.asp version 5.
(19) Sideras, K., Ingle, J. N., Ames, M. M., Loprinzi, C. L., Mrazek, D. P., Black, J. L., Weinshilboum, R. M., Hawse, J. R., Spelsberg, T. C., and Goetz, M. P. (2010) Coprescription of tamoxifen and medications that inhibit CYP2D6. *J. Clin. Oncol. 28*, 2768−2776.
(20) Kotthaus, J., Wahl, B., Havemeyer, A., Kotthaus, J., Schade, D., Garbe-Schönberg, D., Mendel, R., Bittner, F., and Clement, B. (2011) Reduction of N^{ω}-hydroxy-l-arginine by the mitochondrial amidoxime reducing component (mARC). *Biochem. J. 433*, 383−391.
(21) Da Cruz, S., Xenarios, I., Langridge, J., Vilbois, F., Parone, P. A., and Martinou, J. C. (2003) Proteomic analysis of the mouse liver mitochondrial inner membrane. *J. Biol. Chem. 278*, 41566−41571.
(22) Islinger, M., Luers, G. H., Li, K. W., Loos, M., and Volkl, A. (2007) Rat liver peroxisomes after fibrate treatment. A survey using quantitative mass spectrometry. *J. Biol. Chem. 282*, 23055−23069.
(23) Wiese, S., Gronemeyer, T., Ofman, R., Kunze, M., Grou, C. P., Almeida, J. A., Eisenacher, M., Stephan, C., Hayen, H., Schollenberger, L., Korosec, T., Waterham, H. R., Schliebs, W., Erdmann, R., Berger, J., Meyer, H. E., Just, W., Azevedo, J. E., Wanders, R. J., and Warscheid, B. (2007) Proteomics characterization of mouse kidney peroxisomes by tandem mass spectrometry and protein correlation profiling. *Mol. Cell. Proteomics 6*, 2045−2057.
(24) Enemark, J. H., Astashkin, A. V., and Raitsimring, A. M. (2006) Investigation of the coordination structures of the molybdenum(V) sites of sulfite oxidizing enzymes by pulsed EPR spectroscopy. *Dalton Trans.*, 3501−3514.
(25) Hanson, G. R., and Lane, I. (2010) Dimethylsulfoxide (DMSO) reductase, a member of the DMSO reductase family of molybdenum enzymes, in *Metals in Biology, Biological Magnetic Resonance* (Hanson, G., and Berliner, L., Eds.) pp 169−199, Springer, New York.
(26) Enemark, J. H., Raitsimring, A. M., Astashkin, A. V., and Klein, E. L. (2011) Implications for the mechanism of sulfite oxidizing enzymes from pulsed EPR spectroscopy and DFT calculations for "Difficult" Nuclei. *Faraday Discuss. 148*, 249−267.
(27) Enemark, J. H., Astashkin, A. V., and Raitsimring, A. M. (2010) High resolution EPR spectroscopy of Mo-enzymes. Sulfite oxidases: Structural and functional implications, in *Metals in Biology: Applications of High Resolution EPR to Metalloenzymes* (Hanson, G. R., and Berliner, L. J., Eds.) pp 122−169, Springer, New York.
(28) Astashkin, A. V., Enemark, J. H., and Raitsimring, A. (2006) 26.5−40 gHz K_a-band pulsed EPR spectrometer. *Concepts Magn. Reson., Part B 29B*, 125−136.
(29) http://www.thch.uni-bonn.de/tc/orca (version 2.7.0).
(30) Astashkin, A. V., Klein, E. L., Ganyushin, D., Johnson-Winters, K., Neese, F., Kappler, U., and Enemark, J. H. (2009) Exchangeable oxygens in the vicinity of the molybdenum center of the high-pH form of sulfite oxidase and sulfite dehydrogenase. *Phys. Chem. Chem. Phys. 11*, 6733−6742.
(31) Klein, E. L., Astashkin, A. V., Ganyushin, D., Riplinger, C., Johnson-Winters, K., Neese, F., and Enemark, J. H. (2009) Direct detection and characterization of chloride in the active site of the low-pH form of sulfite oxidase using electron spin echo envelope modulation spectroscopy, isotopic labeling, and density functional theory calculations. *Inorg. Chem. 48*, 4743.
(32) Becke, A. D. (1988) Density-functional exchange-energy approximation with correct asymptotic-behavior. *Phys. Rev. A 38*, 3098−3100.
(33) Perdew, J. P. (1986) Density-functional approximation for the correlation-energy of the inhomogeneous electron-gas. *Phys. Rev. B 33*, 8822−8824.
(34) Schäfer, A., Huber, C., and Ahlrichs, R. (1994) Fully optimized contracted gaussian basis sets of triple zeta valence quality for atoms Li to Kr. *J. Chem. Phys. 100*, 5829−5835. Weigend, F., Haeser, M., Patzelt, H., and Ahlrichs, R. ftp://ftp.chemie-karlsruhe.de/pub/basen, 2006.
(35) Schäfer, A., Horn, H., and Ahlrichs, R. (1992) Fully optimized contracted gaussian-basis sets for atoms Li to Kr. *J. Chem. Phys. 97*, 2571−2577.
(36) Pantazis, D. A., Chen, X.-Y., Landis, C. R., and Neese, F. (2008) All-electron scalar relativistic basis sets for third-row transition metal atoms. *J. Chem. Theory Comput. 4*, 908−919.
(37) Klamt, A., and Schuurmann, G. (1993) Cosmo - a new approach to dielectric screening in solvents with explicit expressions for the screening energy and its gradient. *J. Chem. Soc., Perkin Trans. 2*, 799−805.
(38) Sinnecker, S., and Neese, F. (2006) Spin-spin contributions to the zero-field splitting tensor in organic triplets, carbenes and biradicalss - a density functional and *ab initio* study. *J. Phys. Chem. A 110*, 12267−12275.
(39) Baerends, E. J., Ellis, D. E., and Ros, P. (1973) Self-consistent molecular hartree-fock-slater calculations. The computational procedure. *Chem. Phys. 2*, 41−51.
(40) Dunlap, B. I., Connolly, J. W. D., and Sabin, J. R. (1979) Some approximations in applications of x-alpha theory. *J. Chem. Phys. 71*, 3396−3402.
(41) Eichkorn, K., Treutler, O., Ohm, H., Haser, M., and Ahlrichs, R. (1995) Auxiliary basis-sets to approximate coulomb potentials. *Chem. Phys. Lett. 240*, 283−289.
(42) Eichkorn, K., Weigend, F., Treutler, O., and Ahlrichs, R. (1997) Auxiliary basis sets for main row atoms and transition metals and their use to approximate coulomb potentials. *Theor. Chem. Acc. 97*, 119−124.
(43) Vanlenthe, E., Baerends, E. J., and Snijders, J. G. (1993) Relativistic regular 2-component hamiltonians. *J. Chem. Phys. 99*, 4597−4610.
(44) van Wüllen, C. (1998) Molecular density functional calculations in the regular relativistic approximation: Method, application to coinage metal diatomics, hydrides, fluorides and chlorides, and comparison with first-order relativistic calculations. *J. Chem. Phys. 109*, 392−399.
(45) van Lenthe, J. H., Faas, S., and Snijders, J. G. (2000) Gradients in the ab initio scalar zeroth-order regular approximation (ZORA) approach. *Gen. Phys. Chem. 328*, 107−112.
(46) Becke, A. D. (1993) Density-functional thermochemistry. The role of exact exchange. *J. Chem. Phys. 98*, 5648−5652.
(47) Lee, C., Yang, W., and Parr, R. P. (1988) Developement of the colle-salvetti correlation-energy formula into a functional of the electron density. *Phys. Rev. 37*, 785−789.
(48) Kisker, C., Schindelin, H., Pacheco, A., Wehbi, W., Garrett, R. M., Rajagopalan, K. V., Enemark, J. H., and Rees, D. C. (1997) Molecular basis of sulfite oxidase deficiency from the structure of sulfite oxidase. *Cell 91*, 973−983.
(49) Astashkin, A. V., and Raitsimring, A. M. (2000) Refocused primary echo: A zero dead time detection of the electron spin echo envelope modulation. *J. Magn. Reson. 143*, 280−291.
(50) Semin, G. K., Babushkina, T. A., and Iakobson, G. G. (1975) *Nuclear Quadrupole Resonance in Chemistry*, Wiley, NewYork.
(51) Hanson, G. R., Wilson, G. L., Bailey, T. D., Pilbrow, J. R., and Wedd, A. G. (1987) Multifrequency electron spin resonance of molybdenum(V) and tungsten(V) compounds. *J. Am. Chem. Soc. 109*, 2609−2616.
(52) Astashkin, A. V., Neese, F., Raitsimring, A. M., Cooney, J. J. A., Bultman, E., and Enemark, J. H. (2005) Pulsed EPR investigations of systems modeling molybdenum enzymes: Hyperfine and quadrupole parameters of oxo-^{17}O in $[MoO^{17}O(SPh)_4]^-$. *J. Am. Chem. Soc. 127*, 16713−16722.

(53) Matar, K., and Goldfarb, D. (1992) Fourier transform electron spin echo envelope modulation of a S = 1/2, I = 5/2 spin system: An exact analysis and a second order perturbation approach. *J. Chem. Phys. 96*, 6464−6476.
(54) Baute, D., and Goldfarb, D. (2005) The ^{17}O hyperfine interaction in $V^{17}O(H_2{}^{17}O)_5{}^{2+}$ and $Mn(H_2{}^{17}O)_6{}^{2+}$ determined by high field endor aided by DFT calculations. *J. Phys. Chem. A 109*, 7865−7871.
(55) Astashkin, A. V., Johnson-Winters, K., Klein, E. L., Feng, C., Wilson, H. L., Rajagopalan, K. V., Raitsimring, A. M., and Enemark, J. H. (2008) Structural studies of the molybdenum center of the pathogenic R160Q mutant of human sulfite oxidase by pulsed EPR spectroscopy and ^{17}O and ^{33}S labeling. *J. Am. Chem. Soc. 130*, 8471−8480.
(56) Patchkovskii, S., and Ziegler, T. (1999) Prediction of electron paramagnetic resonance g-tensors of transition metal complexes using density functional theory: First applications to some axial d^1MeX_4 systems. *J. Chem. Phys. 111*, 5730−5736.
(57) Cosper, M. M., Neese, F., Astashkin, A. V., Carducci, M. D., Raitsimring, A. M., and Enemark, J. H. (2005) Determination of the g-tensors and their orientations for *cis,trans*-(l-N_2S_2)(MoOX)-O^{-v} (X = Cl, SCH_2PH) by single-crystal EPR spectroscopy and molecular orbital calculations. *Inorg. Chem. 44*, 1290−1301.
(58) Hadt, R. G., Nemykin, V. N., Olsen, J. G., and Basu, P. (2009) Comparative calculation of EPR spectral parameters in $[Mo(V)OX_4]^-$, $[Mo(V)OX_5]^{2-}$, and $[Mo(V)OX_4(H_2O)]^-$ complexes. *Phys. Chem. Chem. Phys. 11*, 10377−10384.
(59) Drew, S. C., Young, C. G., and Hanson, G. R. (2007) A density functional study of the electronic structure and spin hamiltonian parameters of mononuclear thiomolybdenyl complexes. *Inorg. Chem. 46*, 2388−2397.
(60) Fritscher, J., Hrobarik, P., and Kaupp, M. (2007) Computational studies of EPR parameters for paramagnetic molybdenum complexes. Larger Mo^v systems relevant to molybdenum enzymes. *Inorg. Chem. 46*, 8146−8161.
(61) George, G. N., Garrett, R. M., Prince, R. C., and Rajagopalan, K. V. (2004) Coordination chemistry at the molybdenum site of sulfite oxidase: Redox-induced structural changes in the Cysteine 207 to Serine mutant. *Inorg. Chem. 43*, 8456−8460.
(62) Astashkin, A. V., Mader, M. L., Enemark, J. H., Pacheco, A., and Raitsimring, A. M. (2000) Direct detection of the proton-containing group coordinated to Mo(V) in the high-pH form of chicken liver sulfite oxidase by refocused primary ESEEM spectroscopy: Structural and mechanistic implications. *J. Am. Chem. Soc. 122*, 5294−5302.
(63) Astashkin, A. V., Raitsimring, A. M., Feng, C., Johnson, J. L., Rajagopalan, K. V., and Enemark, J. H. (2002) The Mo-OH proton of the low pH form of sulfite oxidase: Comparison of the hyperfine interactions obtained from pulsed ENDOR, CW-EPR and ESEEM measurements. *Appl. Magn. Reson. 22*, 421−430.
(64) Raitsimring, A. M., Astashkin, A. V., Feng, C., Enemark, J. H., Nelson, K. J., and Rajagopalan, K. V. (2003) Pulsed EPR studies of the exchangeable proton at the molybdenum center of dimethyl sulfoxide reductase. *J. Biol. Inorg. Chem. 8*, 95−104.
(65) Astashkin, A. V., Raitsimring, A. M., Feng, C., Johnson, J. L., Rajagopalan, K. V., and Enemark, J. H. (2002) Pulsed EPR studies of non-exchangeable protons near the Mo(V) center of sulfite oxidase: Direct detection of the -proton of the coordinated cysteinyl residue and structural implications for the active site. *J. Am. Chem. Soc. 124*, 6109−6118.
(66) Lamy, M. T., Gutteridge, S., and Bray, R. C. (1980) Electron-paramagnetic-resonance parameters of molybdenum(V) in sulphite oxidase from chicken liver. *Biochem. J. 185*, 397−403.